OCTOBER 22 2024

Computational modeling of phononic pseudocrystal isolators FREE

S. Hales Swift; Chandler B. Smith; Rick A. Kellogg; Ihab F. El-Kady; Jerry W. Rouse

Proc. Mtgs. Acoust. 51, 022007 (2023)
https://doi.org/10.1121/2.0001968

Volume 51 http://acousticalsociety.org/

184th Meeting of the Acoustical Society of America

Chicago, Illinois

8-12 May 2023

Computational Acoustics: Paper 4pCA2

Computational modeling of phononic pseudocrystal isolators

S. Hales Swift
Department of Photonic and Phononic Microsystems, Sandia National Laboratories, Albuquerque, NM, 87114; hales.swift@gmail.com

Chandler B. Smith
Simulation Modeling Sciences, Sandia National Laboratories, Albuquerque, NM, 89123; chasmit@sandia.gov

Rick A. Kellogg
Sandia National Laboratories, Albuquerque, NM, 87123; rakello@sandia.gov

Ihab F. El-Kady
Department of Photonic and Phononic Microsystems, Sandia National Laboratories, Albuquerque, NM, 87123; ielkady@sandia.gov

Jerry W. Rouse
Sandia National Laboratories, Analytical Structural Dynamics, Albuquerque, NM, 87123; jwrouse@sandia.gov

Recent technical efforts at Sandia National Laboratories have identified a need for broadband high-frequency vibration isolation spanning a wide range of ultrasonic frequencies. To fill this need, phononic pseudocrystal isolators based upon a structure with cyclic symmetry and radial self-similarity was developed that can potentially suppress frequency transmission across a range far larger than that observed for normal phononic crystals. To enable calculation of transmission characteristics for these articles, boundary conditions enabling half-channel calculations are proposed and their validity demonstrated for both longitudinal and shear waves. These boundary conditions also apply to conventional phononic crystals and can result in significant savings when properly applied for normal incidence longitudinal and shear waves. Additionally, this paper demonstrates and gives formulas for implementing energy density methods that can be used to track wave extinction within phononic pseudocrystals as well as canonical phononic crystal structures.

Published by the Acoustical Society of America

https://doi.org/10.1121/2.0001968.

1. PROBLEM INTRODUCTION

Isolating specific regions or parts to exclude or contain vibration is important. Whether isolating optics from vibration, separating mechanical power and data channels to prevent mechanical crosstalk,[1] or otherwise containing or excluding vibration in a particular region, the ability to contain vibration within a specified frequency range in a specified region to a specified degree is key.

The present effort originated with a requirement for vibration isolation of 20 dB or more across a "wide" frequency range, wide in this case meaning a suppression range 50% above and below a center frequency, resulting in a ratio between the upper and lower bounds of the suppression range of 3. The geometry of interest for this problem was also roughly annular. Consequently, we opted for an unconventional approach. A pseudocrystal with cyclic symmetry in the circumferential direction, but growing geometrically in the radial direction with row number would allow the resultant structure to fit nicely into an annular footprint, while also blocking a frequency range that would be expected to expand with the ratio between the outer and inner radii. A 2-D example of this family of pseudocrystal configuration is shown in Fig. 1.

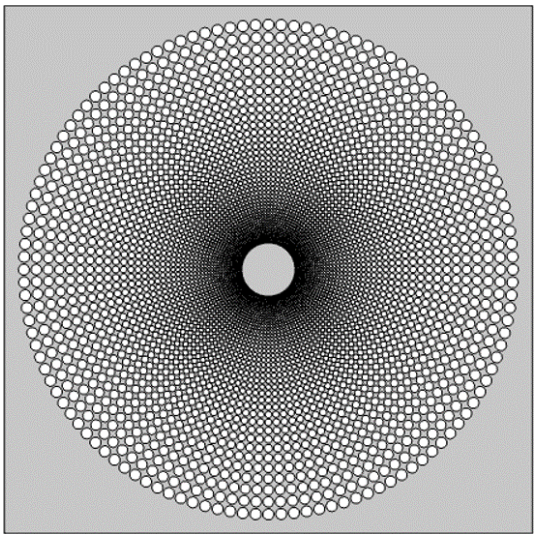

Figure 1: Example annular phononic pseudocrystal with hole size growing geometrically with row number in the radial direction. Case has 120 holes per ring, geometric growth rate 1.05, and filling fraction of 0.42. The size outer-to-inner radii ratio is close to 10.

Conventional phononic crystals are structures that have a strict geometric or material periodicity; in some instances, owing to the pattern of scattering produced, such structures exhibit band gaps: ranges of frequencies at which no wave can propagate (see Ref. 2 for a general review). If a wave were initiated with a frequency within this prohibited range at the crystal boundary it would be reflected with its remnants in the crystal region evanescing. When modeling phononic crystals to find band gaps, a unit cell—the smallest piece of the structure that can completely tessellate (tile) the structure—is identified, and Bloch-Floquet boundary conditions are imposed, which represent the propagation of unattenuated plane waves through the unit cell over the range of unique wavenumbers (representing among other things the possible directions in which waves could be traveling through the material) or, as is more frequently done, the boundary of that set of wavenumbers. The unit cell and the associated boundary is shown in the inset to Fig. 2, where the center Γ, the center of the x side X, and the corner M—the symmetry points that serve as the boundaries for the Bloch-Floquet evaluation—are shown. The eigenmodes and eigenvalues are then evaluated over these wavenumber combinations to determine the allowed modes and their frequencies as shown in Fig. 2. The polarization—the source of the colorization in the plot—is given by

$$P = \frac{\int |u|^2 dV}{\int |u|^2 + |v|^2 dV}$$

and can be used to easily identify longitudinal modes (red) and shear modes (blue) in the dispersion. The total band gaps associated with our unit cell are shown as red rectangles. The calculation process used to produce the band diagram assumes that the unit cell is infinitely repeated, a condition which is, however, never true in nature: phononic crystals are nevertheless known to perform well in suppressing vibration at frequencies *sufficiently* within the band gap if the barrier contains around 5 similar unit cells in the direction of propagation.

In our original design approach, instead of interpreting *similar* to mean *identical* (as in conventional phononic crystals) we interpreted it to mean that unit cells exhibited overlapping band gaps; consequently, after identifying a unit cell with acceptable structural properties (constant filling fraction of 0.42), and a reasonably prominent band gap (upper to lower gap edge frequency ratio of $f_{up}/f_{low} = 1.33$), a growth rate of around 1.05 was selected that allowed the main band gap to overlap for nearly six unit cells ($1.05^6 = 1.34$). Numerical experiments were conducted to determine the vibration suppression effected by this design. Aluminum material properties were used for these simulations.

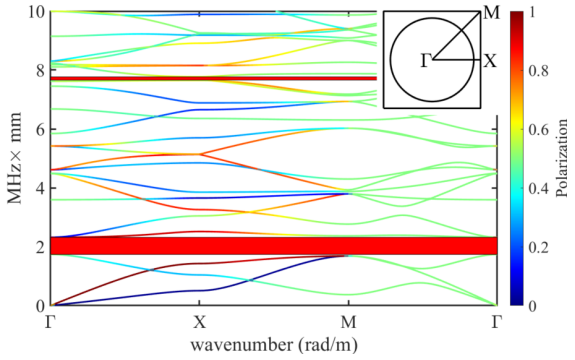

Figure 2: 2-D band structure calculated in COMSOL for a hole in a square unit cell with hole radius equal to 0.43 times the square side length, and the material aluminum.

Contemporary with these numerical experiments, a literature search turned up some 1-D examples of various kinds, but no truly 2-D examples. The reports of the 1-D examples show the ability to affect relatively large ranges of frequencies of surface waves using grooves with "chirped" spacing[3] or acoustics waves traveling through a "chirped" arrangement of cylinders.[4] Radial phononic crystals have also been explored.[5] However, it appears that the abstract and ASA presentation[6] associated with this POMA are the first published results for self-similar 2-D/2.5-D pseudocrystals. Between the initial presentation and the release of this proceedings, further presentations and papers have begun to explore this space.[7–10]

The lack of attention phononic pseudocrystals garnered prior 2023 is due in part to the modeling challenges they pose. The band gaps and performance of canonical phononic crystals are straightforward to calculate because of their exact periodicity. Absent exact periodicity, band structure-type calculations are less straightforward,[11] although the same vibration suppression phenomena *and more* are ultimately achieved. For example, we initially assumed suppression would follow the band gaps associated with the approximate local unit cell. However, an Acoustics (not Solid Mechanics) simulation of the interposer class of Fig. 1 expected by this logic to block a range with an upper-to-lower band edge frequency $r_{ul} < 1.33 \times 1.05^{28} = 5.2$, but the calculated 20^{+}-dB suppression range is closer to 88, 16.9 times that initially expected. With such performance possibilities on the table, methods for predicting the performance of these structures in terms of insertion loss are important. A discussion of the challenges and methods associated with phononic pseudocrystal performance calculations comprise the remainder of this paper.

2. COMPUTATIONAL CHALLENGES AND SOLUTIONS

A. SIZE OF THE UNREDUCED PROBLEM

The key performance characteristic of the phononic pseudocrystal interposer is its insertion loss. Resolving high frequencies necessitates a sufficiently dense grid, preferably with greater than 8 points per wavelength. The solid medium being simulated is aluminum, which has longitudinal and shear wave speeds of 6420 and 3040 m/s, respectively. The shear wave speed is the slower, so properly resolving a given frequency requires a grid element length scale of $l \leq 3040/8f = 380/f$. If the highest frequency of interest were 30 MHz, as could very well be the case for an interposer with a slightly smaller inner radius, the grid would need to be $l \leq 380/30 \times 10^6 = 1.2667 \times 10^{-5}$ m which, if we start with a 10-cm by 10-cm by 3-mm-thick quarter domain as an estimate loosely based on the case shown above, results in something like $0.1 \times 0.1 \times 0.003/(1.2667 \times 10^{-5})^3 = 1.476 \times 10^{10}$ elements (where hex elements have been assumed for ease of calculation), without considering any extra refinement required or savings associated with the holes. Consequently, a direct, brute force approach quickly becomes untenable, particularly for 3-D calculations as the frequency is increased with the associated roughly cubic increase in the required number of elements.

Because of this rapid increase in required resources with volume at high frequency, a number of simplifying approaches are pursued. These efforts to reduce the size of the problem often focus on exploiting symmetries of geometry and scale. Some of these potential exploits are intuitive and easily justified while others require further discussion and assumptions to establish their validity.

B. GEOMETRIC REDUCTIONS OF THE PROBLEM SIZE

i. Half symmetry plane

Among the most easily justified simplifications is a half symmetry plane, shown in Fig. 3. Provided the holes are arranged with a hole or gap toward the side of the planar region receiving excitation, the problem always has at least one natural symmetry plane with regards to both a plane wave proceeding from the left (signified with red arrows) and the interposer, so cutting the domain in half and imposing symmetry on the cut line is—at least for longitudinal waves—a natural choice, allowing immediate simplification. A low-reflecting boundary condition may be applied on the right, with symmetry on the upper side, and a boundary load on the left. Energy density based measures can be applied that consider the ratio of the energy per unit area enclosed by and excluded by the interposer region (see Sec. 3), or transmission loss can be considered (see Sec. 4), though care should be taken in defining the where the associated integrals are evaluated.

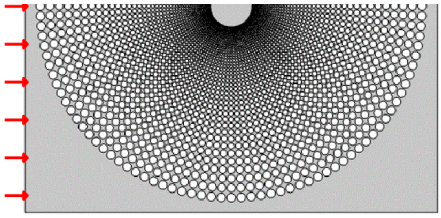

Figure 3: Example half plane case.

ii. Quarter symmetry plane

The quarter-domain shown above requires a bit more justification as it is a more artificial choice. If waves are entering the domain from the left, then waves affecting the back (right) half of Fig. 3 already had a better

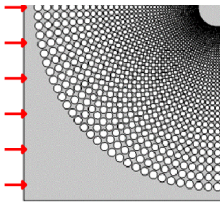

Figure 4: Example quarter plane case.

opportunity to enter through the front (left) half. The shadowed side would not be expected to transmit anything that the first half blocked as the first half already encompasses the range of wave directions encountered in the full geometry; it thus remains a reasonably representative approach that captures all of the possible incoming plane waves that could impinge upon the interposer. We typically imposed a low reflecting boundary condition on the wall on the shadowed side (right side in Fig. 4) to avoid the possible creation of an artificial edge transmission state or trapping vibration within the domain. A cyclic boundary could also be appropriate if the symmetry of the structure supports this (as it does in our case). The cyclic condition would ensure that waves exiting at the lower right corner would re-enter at the upper left going downward instead of rightward, effectively modeling a complete square domain with a complete interposer as in Fig. 1 with plane waves entering from half of each side.

iii. Wedge or channel calculations

Waves that travel within the interposer could be expressed as a family with a radial and circumferential wavenumber on the outer boundary. While the radial wavenumber could assume any desired value, the circumferential wavenumber must be quantized to satisfy cyclic periodicity. Some fraction of the interposer can be modeled and, for allowed circumferential wavenumbers, the result can tessellate the interposer. This would yield a representative set of non-radial waves while reducing the geometry of the problem.

iv. Single-channel calculation

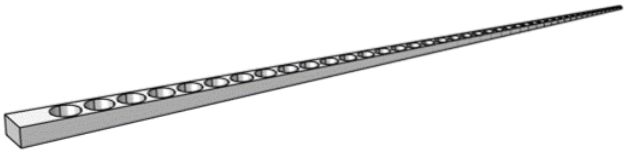

Figure 5: Example single channel case.

Further assumptions enable further reductions. As the outer/inner radius ratio grows, $r_o/r_i >> 1$, the set of initial incoming wave angles that reach the interior shrinks. In the limit, only radial waves need be considered. Consequently, a single channel of holes (as shown in Fig. 5) increasingly becomes a reasonable representative geometry. Cyclic boundary conditions are imposed on the "pie slice cuts", a boundary load is applied on the "crust" end with a low-reflecting boundary condition on the "bite" end. Wave displacements can still be in the radial direction (longitudinal) or in the vertical or circumferential directions (shear modes) when only a single channel is modeled. However, element size limitations remain quite severe during 3-D modeling.

v. Half-channel calculation

The problem can be reduced still further by modeling a half channel and imposing appropriate boundary conditions on both of the sides; however the boundary conditions differ depending on the particular waves being modeled. For longitudinal and vertically polarized shear waves, symmetry boundary conditions, which effectively freeze degrees of freedom normal to the boundary but leave tangential degrees of freedom free, will yield solutions identical to the full channel. For horizontally polarized shear modes, the degrees of freedom normal to the boundary plane need to be left free, while those tangent to the boundary plane need to be frozen. Tangent positions can be frozen using a prescribed displacement in COMSOL referenced to the boundary coordinate system. Consequently, these two groups of waves cannot be calculated with the same boundary conditions. However, the advantage in geometric reduction gained by using a half-channel model

easily leads to scenarios where the reduction in memory and processing requirements would justify the modest hassle of running two different boundary conditions.

vi. Dimensional reduction of the problem

One of the most effective means of reducing the problem size is by calculating performance in 2-D rather than in 3-D. By eliminating thickness as concern, the problem is effectively made infinitely thick in terms of its physical analogue, but 1-element thick in terms of its computational costs. However, 2-D models do not capture all of the relevant physics and, in particular, neglect surface modes, and the effect of thickness on propagation speeds. Nevertheless, this approach can be very useful for analyzing relatively thick interposers where bulk modes would be expected to dominate propagation of energy, and where the propagation direction of incoming waves in precisely known.

3. ASSESSING EXTINCTION THROUGH ENERGY DENSITY

When assessing propagation through a phononic pseudocrystal, it is worth considering which quantity one should calculate in order to assess whether a given wave has been effectively blocked. Certainly amplitude is a popular choice; however, when scattering is present the amplitude may vary strongly in space as standing waves can introduce nodal planes as contributions from incoming and reflected waves cancel one another, and these purely local nodal planes do not imply actual extinction as the amplitude will often recover to its prior heights immediately after such a location. One solution that has been suggested for such effectively reverberant environments is a target state formulated in terms of energy density.[12] At the amplitude nodal plane referenced earlier, there is likely to still be an abundance of motion, so including both the potential (V) and kinetic (T) energy terms effectively assesses whether extinction or something more transitory has occurred.

For the present class of radially self-similar pseudocrystals a further complication can arise when acoustic or elastic energy is concentrated as the radius r decreases because the channel width is shrinking. Inclusion of an $\left(\frac{r}{r_0}\right)^2$ multiplier can account for the shrinking channel; consequently, for the 3-D acoustic case assessing extinction, the energy-based quantity expressed for a time-harmonic field is

$$E = T + V = \frac{1}{2\rho_0 c^2}\left[\frac{1}{k^2}\left(\left|\frac{\partial p}{\partial x}\right|^2 + \left|\frac{\partial p}{\partial y}\right|^2 + \left|\frac{\partial p}{\partial z}\right|^2\right) + |p|^2\right]\left(\frac{r}{r_0}\right)^2, \tag{1}$$

where p is acoustic pressure, r is distance from the center, and r_0 is some reference distance with reference to which results are compared.

A similar expression exists for a 2-D linear elastic material; if $\vec{u} = u\hat{e}_x + v\hat{e}_y + z\hat{e}_z$ is the elastic particle displacement, Y the Young's modulus, ν the Poisson's ratio, and

$$\lambda = \frac{Y\nu}{(1+\nu)(1-\nu)}, \quad \mu = \frac{Y}{2(1+\nu)} \tag{2}$$

are the Lamé parameters, then the comparable elastodynamic expression for a time-harmonic field

is

$$E = T + V = \left(\frac{\rho_0 \omega^2 |\vec{u}|^2}{2} + \frac{\lambda |\nabla \cdot \vec{u}|^2}{2} + \mu \left\{ \left| \frac{\partial u}{\partial x} \right|^2 + \left| \frac{\partial v}{\partial y} \right|^2 + \left| \frac{\partial w}{\partial z} \right|^2 + \frac{1}{2} \left[\left| \frac{\partial u}{\partial y} + \frac{\partial v}{\partial x} \right|^2 + \left| \frac{\partial u}{\partial z} + \frac{\partial w}{\partial x} \right|^2 + \left| \frac{\partial v}{\partial z} + \frac{\partial w}{\partial y} \right|^2 \right] \right\} \right) \left(\frac{r}{r_0} \right)^2. \tag{3}$$

While the radial term mentioned earlier can help in assessing extinction within the phononic crystal, and differentiating this from, e.g., standard radial attenuation effects, the presence of holes effectively alters the the channel width independently and can slightly complicate attenuation assessment. This can be handled by averaging the values on the evaluation line spatially over the local unit pseudocell extent.

In COMSOL, expressions implementing Eqs. 2 and 1 are given, respectively, as

```
0.5*(solid.rho*(2*pi*solid.freq)^2)*(abs(u)^2+abs(v)^2+abs(w)^2)
+solid.lambLame/2*abs(d(u,x)+d(v,y)+d(w,z))^2
+solid.muLame*(abs(d(u,x))^2+abs(d(v,y))^2+abs(d(w,z))^2
+0.5*(abs(d(u,y)+d(v,x))^2+abs(d(u,z)+d(w,x))^2+abs(d(v,z)+d(w,y))^2))
*(x^2+y^2)/r0^2
```

for Solid Mechanics calculations, and

```
(abs(p)^2+1/(2*pi*freq/acpr.c)^2*(abs(px)^2+abs(py)^2+abs(pz)^2))
*(x^2+y^2)/r0^2
```

for Acoustics calculations within COMSOL; in each case the terms in orange may be omitted for 2-D geometry, but should be retained for 3-D geometry. The radial term is given with the assumption that the shape is centered at $(x, y) = (0, 0)$. To energy density values across frequency, a 1D Plot Group containing a Line Graph with a cut line along which to evaluate the expressions can be employed.

4. ASSESSING TRANSMISSION LOSS

Transmission loss (TL) characterizes the difference in acoustic or elastic power that result from an obstruction. While imperfect—e.g., no attempt is made to untangle left- and right-going waves, or near-field effects between the boundary and patterned structure—our measure involved the division of integrals over input and output boundaries or regions with an energy-like argument; specifically,

$$TL = 10 \log_{10} \frac{\int_{in} |f|^2 dA}{\int_{out} |f|^2 dA}, \tag{4}$$

where f is displacement, and the integral is taken over the input and output boundaries. TL Measures based on energy density could also be used; however, we defer further discussion of this idea and other potential issues involved in TL due to space constraints. Our 2-D COMSOL simulations typically implemented a TL measurement in the Definitions area under Variables:

```
PX_in intop1_in(solid.uAmpX*conj(solid.uAmpX)) m³
PX_out intop2_out(solid.uAmpX*conj(solid.uAmpX)) m³
PY_in intop1_in(solid.uAmpY*conj(solid.uAmpY)) m³
PY_out intop2_out(solid.uAmpY*conj(solid.uAmpY)) m³
TL_X 10*log10(PX_in/PX_out)
TL_Y 10*log10(PY_in/PY_out)
```

5. DEMONSTRATIONS

A. 2-D SINGLE-CHANNEL EXAMPLE

A two-dimensional 43-hole channel was modeled using the COMSOL Solid Mechanics interface with holes ranging from a minimum to a maximum radius of 0.2436 mm to 2.0858 mm, respectively, as shown in Fig. 6. Aluminum was modeled as a linear elastic material with longitudinal and shear waves speeds of 6420 m/s and 3040 m/s, respectively, and a density of 2,710 $\mathrm{kg/m^3}$. A free triangular mesh was used. The maximum element growth rate, curvature factor, and resolution of narrow regions parameters were 1.25, 0.3, and 1, respectively. The maximum element size was chosen to be 0.00002 m, which placed some limitations on the frequencies that could be confidently resolved. The total number of (triangular) domain element was 645,844 and boundary elements was 20,320, and the total number of degrees of freedom solved for was 2,623,932.

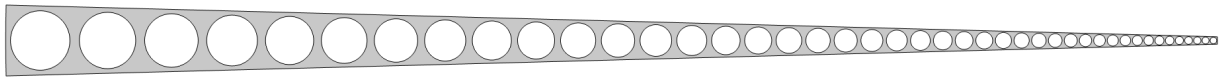

Figure 6: Single-channel geometry with 43 radial holes.

i. Pseudocrystal transmission loss calculation

The transmission loss was evaluated using the expressions from Section 4, and is shown in Fig. 7. The frequencies at which particular minimum numbers of elements per wavelength may be expected based on the designated maximum element size are marked on the plot as vertical lines. The 20-dB suppression line is also marked for visual reference as a dashed red line. For excitation with longitudinal waves, the suppression associated with this design remains above 20 dB (our self-defined suppression target) up to higher frequencies than we can conveniently calculate at even 4 elements per wavelength (the highest frequency shown in the plot). It should be noted that the minimum number of elements per wavelength points are calculated based on the shear wave speed, which is slower than the longitudinal wave speed; this means that for x-direction (longitudinal) excitation, the number of elements per wavelength will be greater than advertised. For excitation with horizontally polarized shear waves, the suppression associated with our design again remains above 20 dB except at 19.53 MHz, when it briefly dips down to 19.6 dB suppression. It is possible that larger dips exist at neighboring or other frequencies. The frequencies evaluated for this study were those between 500,000 Hz and 38,000,000 Hz spaced at 10,000 Hz intervals leaving plenty of possible finer grained variation in transmission overlooked; however, the frequency spacing—rough though it may be in some respects—seems an adequate sampling to characterize the typical suppression produced by this type of design.

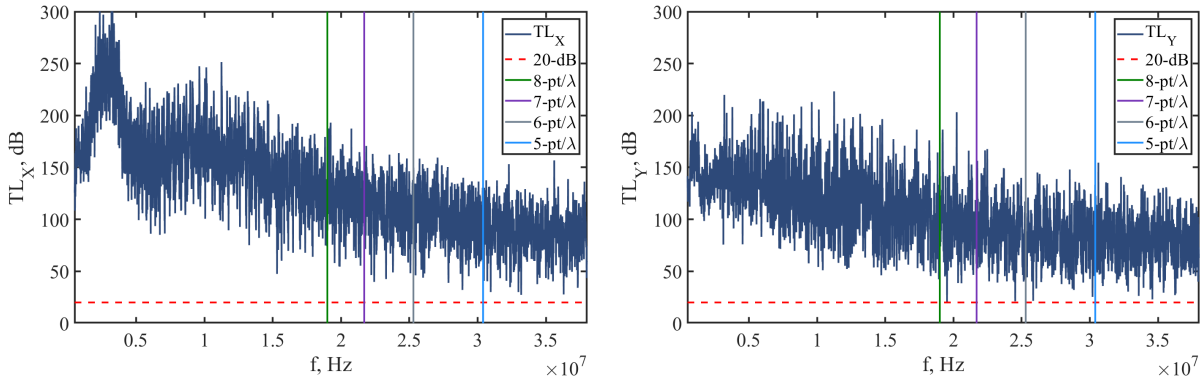

Figure 7: The transmission loss is shown for longitudinal (X), and transverse (Y) excitation of the channel. The frequencies at which particular numbers of finite elements per wavelength are guaranteed based on the designated maximum element size are marked for reference.

ii. Extinction assessment using energy density

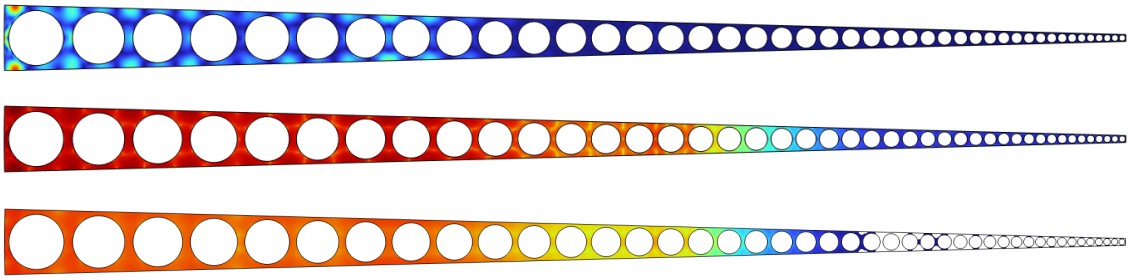

Figure 8: (top) Peak von Mises stress. (middle) Log of peak von Mises stress. (bottom) Log of energy density. Tracking the log of energy density works better for assessing extinction: because it assesses both potential and kinetic energy, energy density is less sensitive to the nulls and peaks produced by local wave interference, enabling greater insight into extinction location.

The procedure described in Section 3 was followed, and energy density was calculated both on a surface for a single frequency for demonstration purposes, and along a cut line at multiple frequencies to provide insight into extinction locations in the present 2-D phononic pseudocrystal model. To show why energy density may be beneficial for tracking the location at which waves become extinct (or evanesce) we here compare with another popular means of visualizing wave phenomenon, the von Mises stress. In Fig. 8 (top), the peak von Mises stress varies a great deal locally while also varying in amplitude over the radius of the channel. The large range of the peak von Mises stress can be visualized more easily by taking the log of this quantity (middle); however, the local variations remain both visible and substantial. The log energy density on the other hand (bottom), because its consideration of both potential and kinetic energy contributions is not as beholden to interference effects as the von Mises stress, can more easily show where particular frequencies are going extinct.

We next consider the extinction of multiple frequencies together using a Line Graph within a 1-D plot group. The approach followed is that outlined in Section 3 toward the end. The cut line is drawn as shown in Fig. 9.

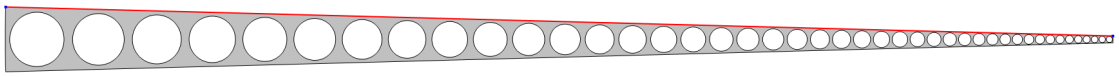

Figure 9: The cut line ran near the upper edge of the channel.

Looking across the collection of frequencies explored and across position along the cut line in Fig. 10, virtually all frequencies of vibration considered experience some attenuation during propagation through the simulated interposer wedge. Some modulation of the energy density by the hole structure is visible as a relatively rapid oscillation with position. Clear frontiers are visible (curved, with increases in frequency with position) at which amplitudes peak and then rapidly decline. The peaking behavior appears to be due to the reflection and consequent constructive interference of waves traveling in the forward and backward directions, after which the portion of the wave within the structure rapidly evanesces.

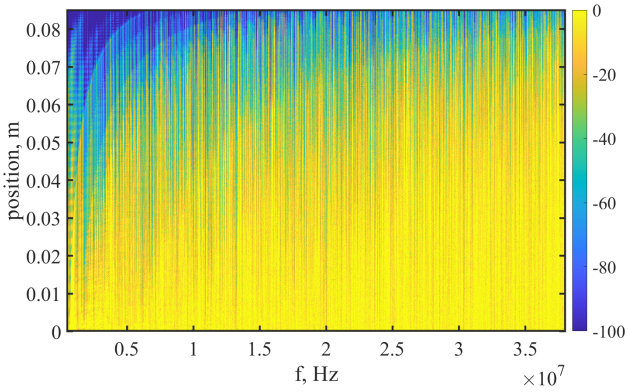

Figure 10: $10\log_{10}$ ***energy density relative to the first (input end) measured cut line station showing extinction of different frequency components as a function of position.***

B. 2-D HALF-CHANNEL EXAMPLE

Figure 11: Half-channel geometry with 43 radial holes.

Following the procedure outlined in section 2.2.5, we repeat the analysis using the half channel shown in Fig. 11. For this example, only the x-direction excitation is considered. Because the excitation and geometry are mirror symmetrical across the x axis, either half may be used in the calculation with symmetry boundary conditions, which fix y-direction displacements while leaving free x-direction displacements. The half channel simulation again uses a maximum element size of 0.00002 m, a minimum element size of 1×10^{-6} m, a maximum element growth rate of 1.25, a curvature factor of 0.3, and resolution of narrow regions parameter of 1. 324,164 domain elements and 10,768 boundary elements are used for a total of 1,318,194 degrees of freedom. These same values held for both the longitudinal and shear excitation cases despite their differing boundary conditions. A piece of the mesh used for this calculation from around the largest hole is shown in Fig. 12; the longitudinal wave transmission loss (evaluated in terms of the x-direction squared amplitudes at the input and output ends of the channel) for the full and half channel cases is shown together in Fig. 13. The input parameters are otherwise the same as in the previous section where a full channel was considered. In order to maximize generality,

Figure 12: A fragment of the mesh surrounding the largest hole in the half-channel case.

no effort was made to ensure that the symmetry boundary was respected in the full channel case. Consequently, minor numerical differences exist in calculated results, but these are typically of small magnitude provided the number of elements per wavelength is large.

Differences in the depth and frequency at which characteristic features occur result from minor differences in meshing, and tend to increase in severity as the number of elements per wavelength decreases. At low frequencies discrepancies tend to be minor. To further illustrate the degree of fidelity between the half-channel and full-channel simulations, we here display the von Mises stress present for a 1 MHz longitudinal excitation through a portion of the structure encompassing the first 8 holes. In each case the half channel result is shown on top adjacent to the bottom of the full channel; below this the full channel is shown intact for visual reference. For

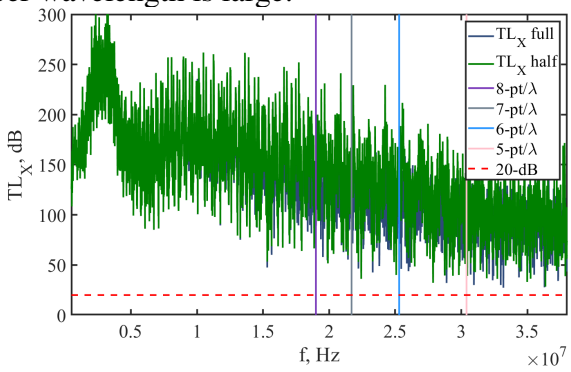

Figure 13: Longitudinal transmission loss with full-channel and half-channel simulation domains.

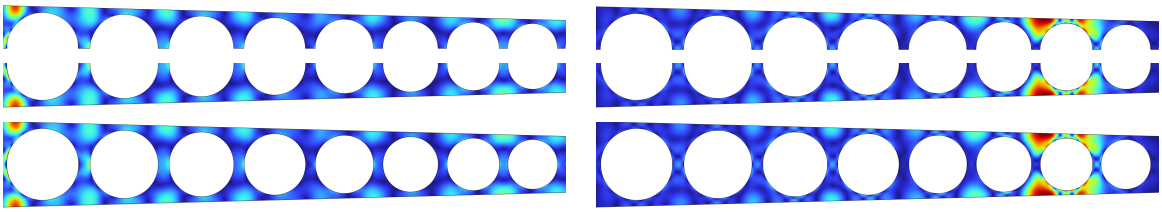

Figure 14: von Mises stress from a 1-MHz longitudinal (left) and a transverse/shear (right) load applied on the left hand side in simulation using a half channel domain (top) and a full channel domain (middle and bottom). Both capture the physics with expected differences only on the level of numerical precision.

both the longitudinal and the horizontally polarized transverse (shear) excitation case, shown in Fig. 14, the half-channel and full-channel calculations yield visually identical results, providing confirmation for our claims regarding the appropriateness of the proposed half-channel boundary conditions.

i. 3-D single-channel example

Because many of the analyses that can be performed for 3-D cases are similar those already shown for 2-D, we will not repeat all of them here. The main challenge with 3-D cases is the size of the mesh which scales as the reciprocal cube of the maximum element size. Consequently, the case we highlight here will utilize a 39-hole half channel (shown in Fig. 15 as this effectively allows us to resolve a frequency a factor of $\sqrt[3]{2}$ of that which we can achieve in a full channel calculation for the same computational expense.

Figure 15: 3-D tapered half-channel geometry.

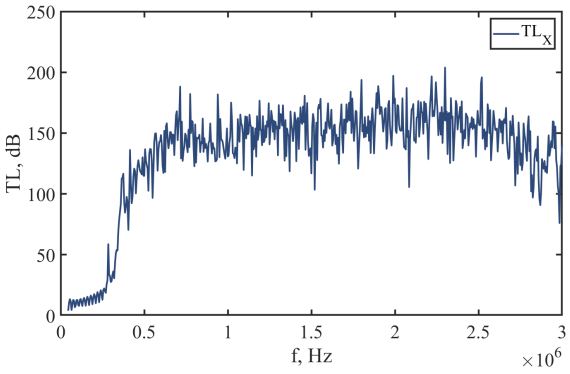

Figure 16: Transmission loss as a function of frequency for our tapered channel.

Our mesh has a maximum element size of $\Delta x_{max-el} = 0.00015$ m, and contains 870,023 domain elements, 84,520 boundary elements, and 5,053 edge elements, resulting in a model with 3,736,872 degrees of freedom. The highest frequency considered in this model is 3×10^6 Hz, and the modeled material is aluminum with the lowest (shear) wave speed 3100 m/s. Consequently, $\lambda_{min} = \frac{3100}{3\times10^6} = 0.00103\bar{}$, and we are guaranteed to have $\frac{\lambda_{min}}{\Delta x_{max-el}} = \frac{0.00103\bar{}}{0.00015} = 6.\bar{8}$ points per minimum wavelength. The longitudinal wave speed, which is the more important for the longitudinal excitation considered here is considerably higher, at 5790 m/s, resulting in a $\lambda = \frac{5790}{3\times10^6} = 0.0019$ m wavelength and, consequently, $\frac{0.0019}{0.00015} = 12.9$ elements per longitudinal wavelength. The transmission loss is evaluated between 45 kHz and 3 MHz and the results are shown in Fig. 16 where it can be seen that, in 3D also, pseudocrystals with cyclic symmetry and radial self similarity can produce suppressed transmission over relatively large frequency ranges. The maximum frequency in the simulation is 3 MHz and the lowest 20-dB-suppressed frequency was 275 kHz; this result implies that suppression over larger ranges ($f_{up}/f_{low} > 10.91$) than those implied by the translation of expected band gap ($f_{up}/f_{low} < 1.33 \times 1.05^3 3 = 8.92$) applies in 3D as well as 2D, and that cyclically symmetrical and radially self-similar phononic pseudocrystals and other structures built along similar principles can be used to create extreme broadband vibration isolation.

6. CONCLUSIONS

This paper (and its associated presentation) introduced a class of phononic pseudocrystals exhibiting cyclical symmetry and radial self-similarity, noted some of their unusual properties such as extreme broadband vibration isolation, and discussed methods for their efficient computation modeling. Boundary conditions were described enabling the modeling of radial longitudinal and both polarizations of shear waves using only half of a radial channel as the computational domain; these boundary conditions differ depending on which group of waves are modeled. Energy density methods were also introduced for the purpose of characterizing the extinction (or evanescing) location of particular frequencies waves within the pseudocrystal domain. Energy density methods are less susceptible to local variations in strain than other common indications of wave motion such as von Mises stress, and as such are helpful for easily visualizing the extinction process. Phononic pseudocrystal isolators exhibit vibration suppression phenomena that extend far beyond the suppression associated with canonical phononic crystals and as such deserve further study.

ACKNOWLEDGMENTS

Sandia National Laboratories is a multi-mission laboratory managed and operated by National Technology & Engineering Solutions of Sandia, LLC (NTESS), a wholly owned subsidiary of Honeywell International Inc., for the U.S. Department of Energy's National Nuclear Security Administration (DOE/NNSA) under contract DE-NA0003525. This written work is authored by an

REFERENCES

[1] C. Sugino, R. Gerbe, E. Baca, C. Reinke, M. Russene, A. Erturk, and I. El-Kady, "Machined phononic crystals to block high-order Lamb waves and crosstalk in through-metal ultrasonic communication systems", *Appl. Phys. Lett.* **120**, 191705 (2022).

[2] M. I. Hussein, M. J. Leamy, M. Ruzzene, "Dynamic of phononic materials and structures: Historical origins, recent progress, and future outlook", *Appl. Mech. Rev.* **66**, 040802 (2014).

[3] Z. Tian, L. Yu, "Rainbow trapping of ultrasonic guided waves in chirped phononic crystal plates", *Sci. Rep.* **7**, 40004 (2017).

[4] V. Romero-García, R. Picó, A. Cebrecos, V. J. Sánchez-Morcillo, and K. Staliunas, "Enhancement of sound in chirped phononic crystals", *Appl. Phys. Lett.*, **102**, 091906 (2013).

[5] D. Torrent, J. Sánchez-Dehesa, "Radial wave crystals: Radially periodic structures from anisotropic metamaterials for Engineering acoustic or electromagnetic waves", *Phys. Rev. Lett.*, **103**, 064301 (2009).

[6] S. H. Swift, C. B. Smith, R. A. Kellogg, I. F. El-Kady, "Modeling the performance of a family of phononic pseudo-crystal interposers", *J. Acoust. Soc. Am.*, **153**, A317 (2023).

[7] S. H. Swift, I. F. El-Kady, R. A. Kellogg, "Principles underlying 2-D phononic pseudocrystal isolators", *Phononics 2023*, PHONONICS-2023-0212 (2023).

[8] C. Dorn, D. M. Kochmann, "Conformally graded metamaterials for wave attenuation", *Phononics 2023*, PHONONICS-2023-0039 (2023)

[9] C. Dorn, D. M. Kochmann, "Conformally graded metamaterials for elastic wave guidance", *Extreme Mech. Lett.*, **65**, 102091 (2023).

[10] B. Telgen, V. Kannan, J.-C. Bail, C. Dorn, H. Niese, D. M. Kochmann, "Rainbow trapping of out-of-plane mechanical waves in spatially variant beam lattices", *J. Mech. Phys. Solids*, **191**, 105762 (2024).

[11] S. H. Swift, "Considering the role of the phononic dispersion relations in understanding the performance of phononic pseudocrystals and similar structures," *J. Acoust. Soc. Am.*, **155**, A192 (2024).

[12] Xu, B., "Generalized Acoustic Energy Density and Its Applications" (2010) *Brigham Young University Theses and Dissertations.* 2339.